

ARTICLE OPEN



Anti-miR-135/SPOCK1 axis antagonizes the influence of metabolism on drug response in intestinal/colon tumour organoids

Roya Babaei-Jadidi^{1,2}, Hossein Kashfi^{1,3}, Walla Alelwani⁴, Ashkan Karimi Bakhtiari¹, Shahad W. Kattan^{1,5}, Omniah A. Mansouri⁶, Abhik Mukherjee⁷, Dileep N. Lobo^{8,9} and Abdolrahman S. Nateri¹✉

© The Author(s) 2022

Little is known about the role of microRNAs (miRNAs) in rewiring the metabolism within tumours and adjacent non-tumour bearing normal tissue and their potential in cancer therapy. This study aimed to investigate the relationship between deregulated miRNAs and metabolic components in murine duodenal polyps and non-polyp-derived organoids (mPOs and mNPOs) from a double-mutant *Apc*^{Min}*Fbxw7*^{ΔG} mouse model of intestinal/colorectal cancer (CRC). We analysed the expression of 373 miRNAs and 12 deregulated metabolic genes in mPOs and mNPOs. Our findings revealed miR-135b might target *Spock1*. Upregulation of SPOCK1 correlated with advanced stages of CRCs. Knockdown of miR-135b decreased the expression level of SPOCK1, glucose consumption and lactic secretion in CRC patient-derived tumours organoids (CRC tPDOs). Increased SPOCK1 induced by miR-135b overexpression promoted the Warburg effect and consequently antitumour effect of 5-fluorouracil. Thus, combination with miR-135b antisense nucleotides may represent a novel strategy to sensitise CRC to the chemo-reagent based treatment.

Oncogenesis (2022)11:4; <https://doi.org/10.1038/s41389-021-00376-1>

INTRODUCTION

The control of nutritional uptake and metabolic pathway activity is required for maintaining intestinal homeostasis and intestinal stem and progenitor cell behaviours [1–3]. Specific cancer-associated mutations enable cells to acquire and metabolise nutrients conducive to proliferation rather than efficient adenosine triphosphate (ATP) production [4–6]. Lactate, glucose, and glutamine act as upstream regulators of oxygen and pH, and are considered important onco-metabolites [7, 8], with tumour cells taking up high amounts of glucose and producing large volumes of lactate even in the presence of oxygen. This process is also known as the “Warburg effect or aerobic glycolysis” [8, 9]. As a result, metabolic heterogeneity between and within human tumours poses a considerable challenge for developing anti-cancer therapies, including against intestinal/colorectal cancer (CRC).

Intestinal/colorectal histologically healthy tissues adjacent to the tumour are commonly used as controls in cancer studies. According to The Cancer Genome Atlas (TCGA) protocols (<http://cancergenome.nih.gov/>), histologically normal tissue adjacent to the tumour (NAT) samples must be collected >2 cm from the tumour margin and/or must not contain tumour [10]. Previously, several studies reported that the tissue-free tumour regions

surrounding the tumour have many morphologic and phenotypic differences from non-tumour-bearing healthy tissue, including pH levels, allelic imbalance and telomere length, stromal behaviour, and transcriptomic and epigenetic aberrations [10–12]. However, little is known about the significance of the metabolic pathways and the molecular mechanism of control of onco-metabolites, especially, the intestinal miRNAs regulated in response to metabolic alteration [13–15] required for promoting neoplastic tissue in the regions immediately surrounding tumours. Therefore, elucidating the molecular mechanisms that orchestrate cellular transformation in these diverse cells and tissues may answer critical biological questions about early tumour formation and lead to identifying new therapeutic targets.

The *APC* (Adenomatous polyposis coli) and *FBXW7* (F-Box and WD repeat domain containing 7) genes are critical tumour suppressors and are amongst the most commonly mutated genes in CRC [16–19]. We and others have previously reported rapid development of adenomas throughout the small and large intestine in *Apc*^{Min}*Fbxw7*^{ΔG} double-mutant mice (*Fbxw7*-deletion in the *Apc*^{Min} background) [20–22]. Tumours start to develop at 2–3 weeks, and mice usually die by 4–5 weeks of age. In contrast, tumours in control *Apc*^{Min} or *Apc*^{Min}*Fbxw7*^{fl/fl} mice do not usually

¹Cancer Genetics & Stem Cell Group, BioDiscovery Institute, Translational Medical Sciences Unit, School of Medicine, University of Nottingham, Nottingham NG7 2UH, UK.

²Respiratory Medicine, School of Medicine, University of Nottingham, Nottingham NG7 2UH, UK. ³Department of Molecular Oncology, H. Lee Moffitt Cancer Center & Research Institute, Tampa, FL, USA. ⁴Department of Biochemistry, College of Science, University of Jeddah, Jeddah, Saudi Arabia. ⁵Medical Laboratory Department, College of Applied Medical Sciences, Taibah University, Yanbu, Saudi Arabia. ⁶Department of Biology, University of Jeddah, College of Science, Jeddah 21959, Saudi Arabia. ⁷Histopathology, BioDiscovery Institute, School of Medicine, University of Nottingham, NG7 2UH, Nottingham, UK. ⁸Nottingham Digestive Diseases Centre, National Nottingham Digestive Diseases Centre, National Institute for Health Research Nottingham Biomedical Research Centre, Nottingham University Hospitals NHS Trust and University of Nottingham, Nottingham, UK. ⁹MRC Versus Arthritis Centre for Musculoskeletal Ageing Research, School of Life Sciences, University of Nottingham, Queen's Medical Centre, Nottingham, UK.

✉email: a.nateri@nottingham.ac.uk

Received: 5 August 2021 Revised: 7 December 2021 Accepted: 15 December 2021

Published online: 19 January 2022

appear until 6 weeks, and death occurs at 18–24 weeks [22, 23]. Both APC and FBXW7 are involved in regulating transcription factors, including c-MYC [24], c-JUN [25], MCL1 (Myeloid Leukemia 1) [26], ZEB2 [27], NOTCH [28], HIF-1 (hypoxia-inducible factor-1) [29], which may be reprogramming cellular metabolism in APC and FBXW7 deficient cells. Interestingly, the miRNA-mediated modulation of APC and FBXW7 genes has also been found to regulate features of cellular transformation, while many miRNAs also function downstream of these transcription factors [16, 17, 30]. However, recent clinical and preclinical studies suggest that the abundance of these proteins and miRNAs, and the outcome of these alterations are sometimes tissue- and cell type-specific.

Moreover, previous data showed that the functional fate of differentiated cell types in intestinal organoids are intrinsically programmed with their specific stem cell location and retain characteristics of their site of origin in culture [31]. Consequently, differential expression of metabolic genes reported as site-specific for rapid tumour growth in the *Apc^{Min}Fbxw7^{ΔG}* double-mutant mice [20, 22], could be detected in murine duodenal polyp-derived organoids (mPOs) versus the adjacent non-polyp-derived organoids (mNPOs) cultures. It is, therefore, important to study this for rapid tumour growth in the *Apc^{Min}Fbxw7^{ΔG}* double-mutant mice in a 3D multiparameter readout. Intestinal organoids are an experimental model, which combines the advantage of producing the entire diversity of crypt epithelial cells in vitro, with relatively quick biomass production and ease of handling. They are an excellent experimental platform to explore the complexity of intrinsic epithelial cell defects. However, until recently, only a few studies dealt with identifying the metabolites in intestinal organoid cultures [1, 2, 32–36]. Therefore, the aim of the present study was to investigate the discrimination between genetically murine *Apc^{Min}Fbxw7^{ΔG}* double-mutant alterations in tumours and matched normal tissue-derived organoids through a possible differential glucose consumption and lactate production, and analyse previously well-known metabolic associated miRNAs.

RESULTS

Duodenal *Apc^{Min}Fbxw7^{ΔG}* double-mutant polyps showed increased glucose consumption and lactate production versus non-polyp organoids

Adenocarcinoma is the most common type of small intestine cancer, and most of these tumours occur in the duodenum, the closest part of the small intestine to the stomach. Therefore, to concordantly analyse glucose and lactate metabolism profiles from small polyps and non-polyp sections, we first developed organoids from dissected duodenum and histologically non-tumour bearing tissues to the tumour, respectively, and from two littermates of three separate breeding pairs from *Apc^{Min}Fbxw7^{ΔG}* double-mutant mice (6× Male, 20 days of age) (Fig. 1A, B). To exclude the possible impact of Wnt3a and Noggin on cellular metabolism [37] between duodenal mNPOs and mPOs culture, we included secreted Noggin in both mNPOs and mPOs cultures. Next, we measured the concentrations of glucose and lactate in the medium for the primary (first passage) organoids, as previously described [38] (Fig. 1C, D).

Through this analysis, we identified strong differences between the metabolism of duodenal mNPOs and mPOs. mPOs had a significantly higher glucose consumption rate (Fig. 1C) and lactate production (Fig. 1D) than mNPOs, indicating a metabolic shift towards anaerobic glycolysis to sustain the higher rate of mPOs growth and derivation of new cancer cells.

Furthermore, in line to validate the conclusion obtained from the above metabolic assay, mRNA expression of a panel of twelve metabolic genes reported as highly deregulated in murine mutated *Apc* tumours [6, 39, 40] was analysed by qRT-PCR. The selected genes involved in cellular metabolism (glucose,

reactive oxygen species (ROS), fatty acid uptake and tissue remodelling). For example, *Aldob* that encodes Aldolase B enhances fructose metabolism and drives metabolic reprogramming of colon cancer liver metastasis [41]. *G6pc* (G6pt) encodes glucose-6-phosphatase and a loss and decrease the level of the glucose-6-phosphatase involved in rat colon carcinomas [42]. *Hexll* encodes Hexokinase 2, which is a key mediator of aerobic glycolysis, provides the tumour with a metabolic advantage over its normal tissue of origin [43]. *Spock1* (a.k.a. Testican-1), an extracellular matrix protein that is conjugated with one or more covalently linked carbohydrate residues, affects colorectal cancer development [44]. *Spock2* (a.k.a. Testican-2), which binds with glycosaminoglycans to form part of the extracellular matrix, may play a role in colorectal carcinogenesis [45]. Glutathione S-transferase theta 1 gene (*GSTT1*) catalyses the conjugation of reduced glutathione to a variety of electrophilic and hydrophobic compounds and may play a role in colorectal carcinogenesis [46]. *Cyba* (a.k.a. CGD4) encodes the alpha subunit, of cytochrome b, a component of the NADPH oxidase (NOX) complex, responsible for the respiratory burst in phagocytes, and has been identified as a potential tumour suppressor gene in breast cancer [47]. *Ephx2* (a.k.a. SHE), encodes the epoxide hydrolase 2, which binds to specific epoxides and converts them to the corresponding dihydrodiols. Mutations in the EPHX2 gene have been associated with familial hypercholesterolaemia [48]. *Fabp6* (a.k.a. ILBP), a transporter whose elimination by ileal resection increases tumour incidence, suggests that malabsorption of bile acids enhances colon tumorigenesis [49]. *Slc2a1* (a.k.a. SGLT1), functions as a mediator of dietary glucose and galactose uptake from the intestinal lumen. Mutations in this gene have been associated with glucose-galactose malabsorption [50, 51]. *Slc2a2* (a.k.a. GLUT2), encoding an integral plasma membrane glycoprotein, acts as a glucose sensor and may play a role in colorectal carcinogenesis [52].

The qRT-PCR analysis highlighted the expression levels of *Aldob*, *Cyba*, *Hexll*, *Fabp6*, *Slc2a5* and *Spock1*, *Spock2* were upregulated, whereas *G6pc*, *Slc2a1* and *Slc2a2* were downregulated but the *Ephx2* and *Gstt1* were unchanged in mPOs versus mNPOs (Fig. 2A). Western blot analysis of SPOCK1 and SPOCK2 protein expression confirmed the induction observed on mRNA levels. SPOCK1 and SPOCK2 proteins (Fig. 2B, C). These data suggest a differential glucose/lactate alteration and metabolic gene expression between duodenal mNPOs and mPOs cells. SPOCK1 carries both heparan and chondroitin sulfate chains, while in contrast, SPOCK2 is a pure heparan sulfate proteoglycan, suggesting that there are specific physiological roles for each SPOCK. SPOCK1 is a positive downstream regulator of TGF- β [53], and expression is regulated through the Wnt/ β -catenin pathway [54]. In addition to its physiological functions, SPOCK1 is a critical regulator in many kinds of cancers, including CRC [55–57]. Therefore, SPOCK1 is a critical regulator in cancer progression.

Differential expression of cancer-associated miRNAs in murine duodenal *Apc^{Min}Fbxw7^{ΔG}* double-mutant POs versus NPOs

As outlined above, in addition to aberrant activity of the transcription factors, other regulators, including miRNAs, can simultaneously be associated with altered metabolic gene expression and their activity in mutated APC and FBXW7 cells. To identify miRNAs during the process of tumorigenesis in polyps and possibly not in non-polyp organoids, we performed a comparative miRNAs expression profiling between duodenal mNPOs and mPOs cultures using the miRCURY LNA miRNA assay [58]. This LNA™-based-system is designed for sensitive and accurate detection of miRNAs expression by qRT-PCR using SYBR-green. The miRNAs expression ($2^{-\Delta\Delta CT}$) were normalised and statistically analysed using Exiqon-GenEx-qPCR analysis software [59]. We compared miRNA expression profiles between duodenal mNPOs and mPOs (Fig. 3A), while excluding differentially expressed miRNAs within the same organoid types

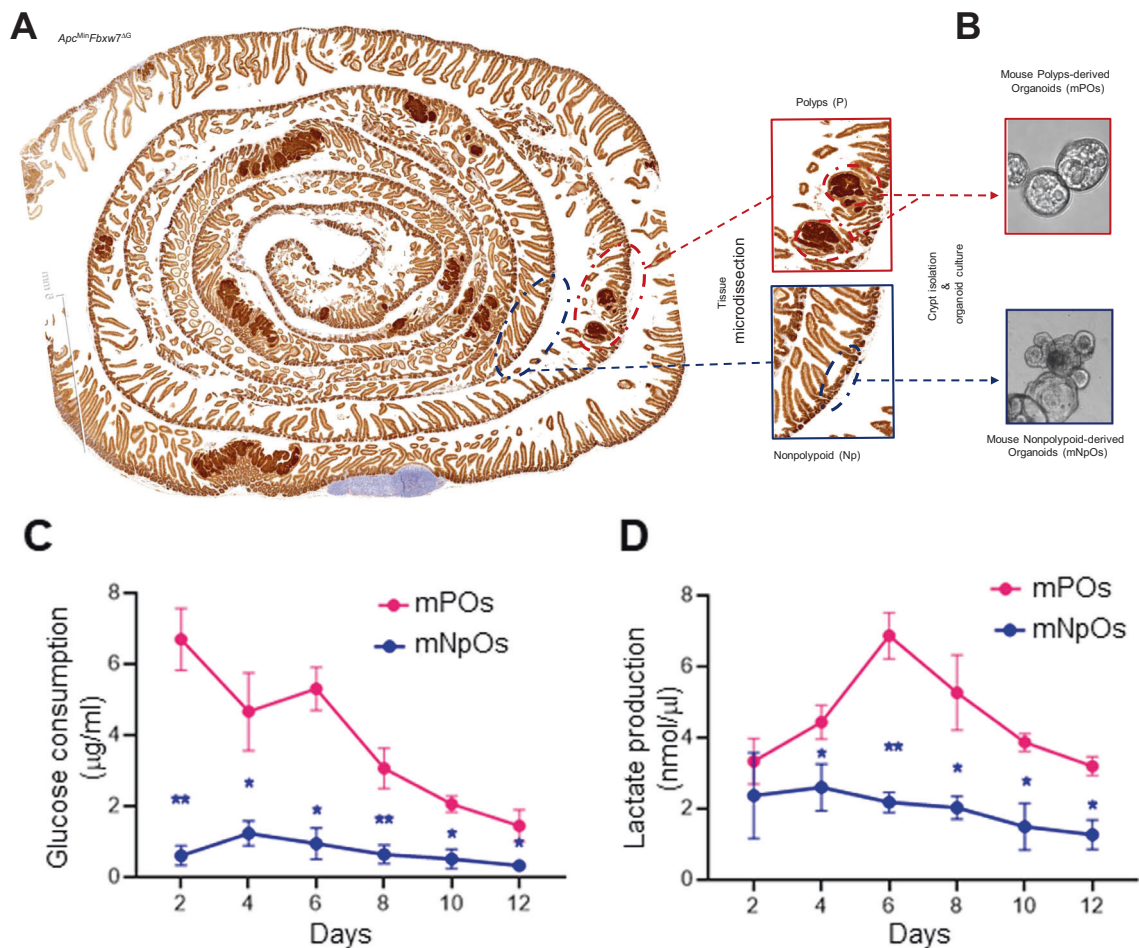


Fig. 1 Murine duodenal *Apc^{Min}Fbxw7^{ΔG}* polyps-derived organoids (mPOs) versus non-polyps-derived organoids (mNPOs) cultures significantly increased glucose consumption and lactate production. **A** Intestinal tumour development of 3 weeks double-mutant *Apc^{Min}Fbxw7^{ΔG}* mice. Dashed lines indicate intestinal polyps (red) and healthy non-polypoid (blue) dissected for mPO and mNPOs cultures. Bar, 100 μm. Boxes indicate magnified the selected intestinal polyps and non-polypoid crypts. **B** Representative live images of duodenal organoids grown for 5 days from isolated polyps and non-polyps crypts. **C** Murine duodenal *Apc^{Min}Fbxw7^{ΔG}*-POs had a significantly higher glucose consumption rate, and lactate production (**D**) than duodenal *Apc^{Min}Fbxw7^{ΔG}*-NPOs, indicating a metabolic shift towards anaerobic glycolysis. The consumed glucose (μg/ml) was calculated by subtracting the medium glucose at each time point (2 to 12 days) from fresh media glucose. The lactate concentration (nmol/μl) was calculated in the medium at each time point (day 2 to day 12). Experiments were performed in six-well plates, seeded ~200 organoids/well for each organoid type, and repeated on at least three independent occasions using three separate litters just about 3 weeks born by different times and different breeding (Male *Apc^{Min}Fbxw7^{ΔG}* X Females *Fbxw7^{fl/fl}*) pairs. Results were normalised to the level of glucose and lactate of each organoid type medium. ($n = 3$; * $P < 0.05$; ** $P < 0.01$).

developed from different litters (Fig. 3B, C). We identified several cancer-associated miRNAs, which were differentially expressed in the mPOs when compared with the mNPOs. Intriguingly, we were able to confirm the significant downregulation of several miRNAs including let-7 family members, as well as a significant upregulation (>3-fold up) of 13 overexpressed miRNAs in mPOs versus mNPOs (Fig. 3A, D). These upregulated miRNAs were: miR-128, miR-135b, miR-136, miR-25, miR-367, miR-26a, miR-425, miR-210, miR-141, miR-30e, miR-103, miR-302 and miR-682 (Fig. 3D, red).

The miR-135 targets the metabolic mediator extracellular matrix glycoprotein *SPOCK1*

Next we explored if any of the overexpressed miRNAs (miRNAs miR-128, miR-135b, miR-136, miR-25, miR-367, miR-26a, miR-425, miR-210, miR-141, miR-30e, miR-103, miR-302 and miR-682) in mPOs vs mNPOs were systematically a target of the metabolic genes (Aldob, Cyba, Hexll, Slc2a1, Slc2a2, Slc2a5, Spock1, Spock2, Ephx2, Gstt1, G6pc and Fabp6) using the TargetScan web server [60]. Based on this analysis, among other above genes, we found *Spock1* was the potential target of miR-135 and, *Spock2* was the

potential target of miR-26a and miR-141 (data not shown). We then found increased expression of *SPOCK1* (Fig. 4A) but not *SPOCK2* (Fig. 4B) was associated with poor overall survival (OS) in human colon adenocarcinoma (COAD). Further stage plot analysis indicated an elevated expression of *SPOCK1* [44], across COAD cancer stages, relatively the highest expression in advanced stages (Fig. 4C).

Murine *Spock1* 3'UTR binding sites for miR-135 were significantly conserved among vertebrates, including humans (Fig. S1). Interestingly, our systematic search analysis for predicted miR-135-5p showed that over hundreds of 670 total predicted genes were associated with cellular metabolism (glucose, reactive oxygen species, metabolism, fatty acid uptake and tissue microenvironment) (Table S1, coloured in green). With this observation, previous studies also demonstrated that inhibition of miR-135b in CRC mouse models reduced tumour growth by controlling genes involved in proliferation, invasion and apoptosis [61], and can be used as a noninvasive biomarker for the detection of CRC and advanced adenoma [62]. Therefore, next, we tested patient-derived organoids (PDOs) as these represent a clinically relevant

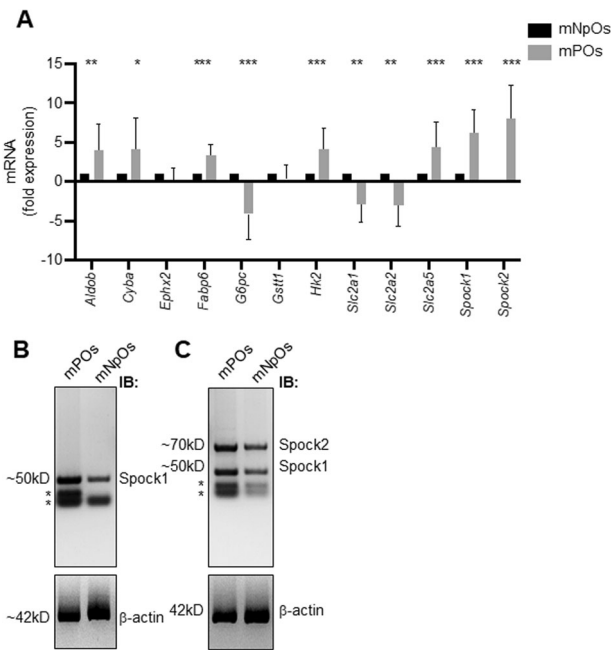


Fig. 2 The murine duodenal *Apc*^{Min}*Fbxw7*^{ΔG}-POs culture conditions compare to the duodenal *Apc*^{Min}*Fbxw7*^{ΔG}-NPOs, impact intestinal organoid cell expression selected metabolic genes. **A** qRT-PCR analysis of mRNA encoding the indicated genes responsible for intestinal metabolism of duodenal *Apc*^{Min}*Fbxw7*^{ΔG}-POs and *Apc*^{Min}*Fbxw7*^{ΔG}-NPOs organoid cells after the 48 h incubation period. Experiments were performed in triplicate for each organoid type from three separate litters samples as outlined in Fig. 1. Results were normalised to β-actin in the same sample, and an average expression data from mPOs samples are presented as fold-induction/repression over mNPOs. Mean ± SE ($n = 3$; * $P < 0.05$; ** $P < 0.01$; *** $P < 0.001$). **B**, **C** Western blot analysis of mPOs and mNPOs organoid proteins using antibodies against Spock1, Spock2, and the loading control β-actin. Experiments were performed on at least two independent occasions.

platform. We and others cultured tumour patient-derived organoids (tPDOs) and adjacent healthy patient-derived organoids (hPDOs) [63–66]. We performed qRT-PCR analysis to investigate the relative expression level of miR-135b and *SPOCK1* in CRC PDOs. We found that expression of *SPOCK1* mRNA (Fig. 4D), and the level of miR-135b expression in CRC tPDOs was significantly higher than in CRC hPDOs (Fig. 4E).

To investigate the regulatory roles of miR-135b on *SPOCK1* expression level, we transduced tPDOs with control vector lentivirus (Control) or miRZip-135b (anti-miR-135b) lentivirus. We then validated that anti-miR-135b significantly decreased the level of miR-135b in CRC tPDOs (Fig. 5A). To confirm the miR-135b/*SPOCK1* axis affects metabolism in tPDO, we tested the concentration of important onco-metabolites: lactate and glucose from the organoid medium treated with anti-miR-135b. Anti-miR-135b was found to decrease glucose consumption and lactate production (Fig. 5B, C). Furthermore, to confirm the miR-135b/*SPOCK1* transcriptionally regulatory axis, we inserted the wild type or mutant 3'UTR of *SPOCK1* (Fig. 5D), into the reporter construct (pEZXTM06 vector) followed by dual-luciferase reporter assays. We found that co-transfection with anti-miR-135b significantly repressed the luciferase activities of cells that contained wild-type *SPOCK1* 3'UTR-reporter but not the mutant *SPOCK1* 3'UTR-reporter (Fig. 5E). Furthermore, qRT-PCR analysis of *SPOCK1* and *SPOCK2* expression confirmed the specificity of repression *SPOCK1* on mRNA levels by suppressing miR-135b expression in CRC tPDOs (Fig. 5F). We demonstrated that *SPOCK1* was the target of miR-135b, and treatment with anti-miR-135b was able to decrease the *SPOCK1* expression.

Inhibition of miRNA-135/*SPOCK1* axis sensitised tPDOs cells to 5-FU-induced cytostatic effects and cytotoxicity

There is extensive information about the role of *SPOCK1* in the tumour extracellular matrix (ECM) dynamic homeostasis process, which activates many molecular signalling pathways (such as EMT process, Wnt/β-catenin, PI3K/Akt and mTOR/S6K signalling pathways) [53, 55, 57, 67]. There is, however, a need for further studies that interrogate this protein as a potential therapeutic target in cancer. Interestingly, some of the recent studies suggest knock-down of *SPOCK1* inhibits the proliferation and invasion in colorectal cancer cells in vitro and in vivo [57, 68]. Notably, a significant upregulation of miR-135b was also previously reported in CRC cell lines and serum of patients with CRC [69]. Therefore, we performed 5-FU (5-fluorouracil) cytostatic and morphological assays (Fig. 6A), on anti-miR-135b expressing tPDOs. Interestingly, we found that combination treatment with miRZip-135b sensitised tPDOs cells to 5-FU-induced cytostatic effects (Fig. 6A, B) and additively repressed the *SPOCK1* gene expression (Fig. 5C).

In addition, we assessed the survival of synchronised/serum-starved human APC-mutated colorectal cancer cell line DLD-1 versus CCD-841 normal colon cells after treatment with ten increasing doses of 5-FU ± anti-miR-135 by SRB colorimetric assay (Fig. 6D). The results indicated that 5-FU exhibits greater cytotoxicity in DLD-1 – anti-miR-135 ($IC_{50} = 10.86 \pm 1.135$), compared to CCD-841 – anti-miR-135 cells ($IC_{50} = 17.48 \pm 1.083$), and miR-135b-knocked down (+anti-miR-135) sensitises colon cancer DLD-1 cells greater than non-cancerous (CCD-841) cells [DLD-1 + anti-miR-135 ($IC_{50} = 5.383 \pm 1.188$) vs CCD-841 + anti-miR-135 cells ($IC_{50} = 14.07 \pm 1.103$)]. Selectivity Index (SI) was calculated by dividing the IC_{50} of – anti-miR-135 cells by the IC_{50} of miR-135b-knocked down cells (DLD-1 SI = 2.017 vs CCD-841 SI = 1.242). SI is an index that gives an idea about selectivity, and the highest value indicates a more selective candidate. Our data are in line with the observations that miR-135 inhibition affects the resistance to chemotherapeutic agents in cultured CRC cell lines [69, 70].

DISCUSSION

A growing body of work has identified several metabolic pathways necessary for enterocytes and gastrointestinal stem cells to function during homeostasis [1, 2, 32]. Metabolic reprogramming has also been widely accepted as a distinct hallmark of intestinal/colorectal tumorigenesis [71, 72]. In these contexts, healthy and cancer epithelial cell metabolism constitutes an initial checkpoint between diet and the fate and phenotype of the host cells, and how these cells interact with other cells and the microenvironment. In addition, this metabolic reprogramming is an active process governed by oncogenes, and tumour suppressors are critical in cancer initiation and shaping the response of colorectal cancer cells to chemotherapy [32, 73–77]. Interestingly, a recent effort through differential expression analyses across tissue types, clearly observed that several metabolic genes and pathways define the mechanism of divergence between healthy tissue adjacent to tumour [10, 78]. While altered metabolism has long been recognised as a central hallmark of cancer, we have only recently begun to elucidate a mechanistic understanding of CRC metabolism. Thus, it is important to study the significance and mechanism of histologically metabolic variation in intestinal tumours and adjacent healthy tissue.

Previous works showed that mutated FBXW7 and APC proteins display a gain-of-function feature to adapt to the environment by reprogramming metabolic pathways via targeting WNT signalling, MYC, mTOR, HIF-1, SREBP (cholesterol and fatty acid synthesis), PRMT5 (protein arginine methyl-transferase 5) transcription and epigenetic factors [79–84]. Since APC and FBXW7 are frequently mutated in CRC, it is important to investigate further the coordination between their mutated activities and cellular

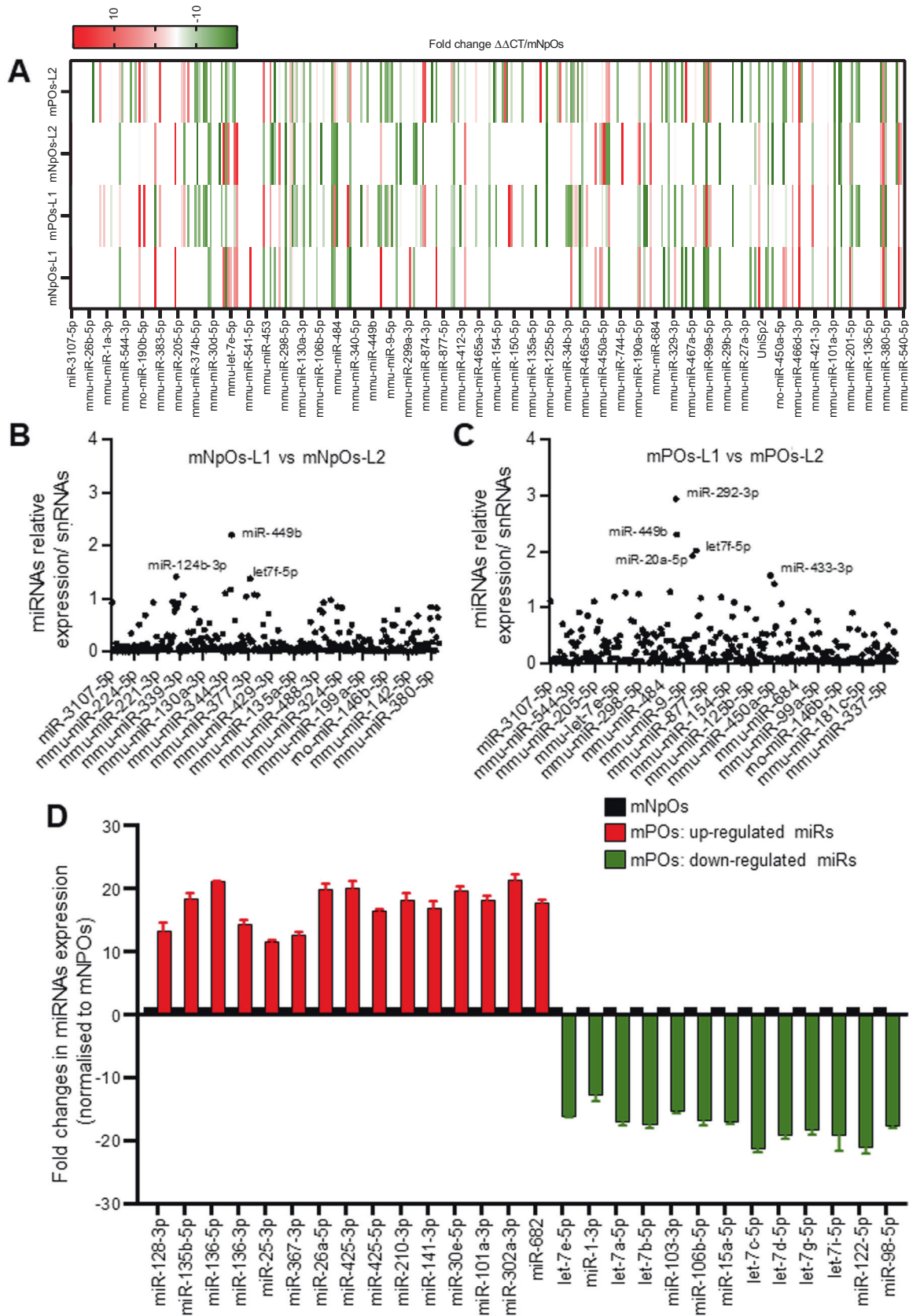


Fig. 3 Comparison of miRNA expression fold changes in duodenal *Apc*^{Min}*Fbxw7*^{ΔG}-POs compared to *Apc*^{Min}*Fbxw7*^{ΔG}-NPOs. **A** Heat-map representation of the 384 differentially expressed miRNAs in mPOs litter 1 (mPOs-L1) and mPOs litter 2 (mPOs-L2) vs mNPOs obtained from the miRCURY-LNA- SYBR Green-PCR-system. Each column represents a miRNA, and not all miRNAs (row labels) could be named. Colour code within the graph represents relative expression; green, downregulated and red, upregulated. **B, C** Differentially expressed miRNAs between mPOs and between mNPOs form two different litters, which the named miRNAs over 1.5 thresholds are excluded for further study. **D** Fold changes of differential expression levels of 28 miRNAs obtained from the screening (**A**) were confirmed by RT-qPCR analysis in organoids. Experiments were performed in triplicate for each organoid type, form three separate litters samples as outlined in Fig. 1. Error bars represent SEM, and one miRNA with a *P* value of 0.001 or less is 3 or higher fold increased (red) or decreased (green).

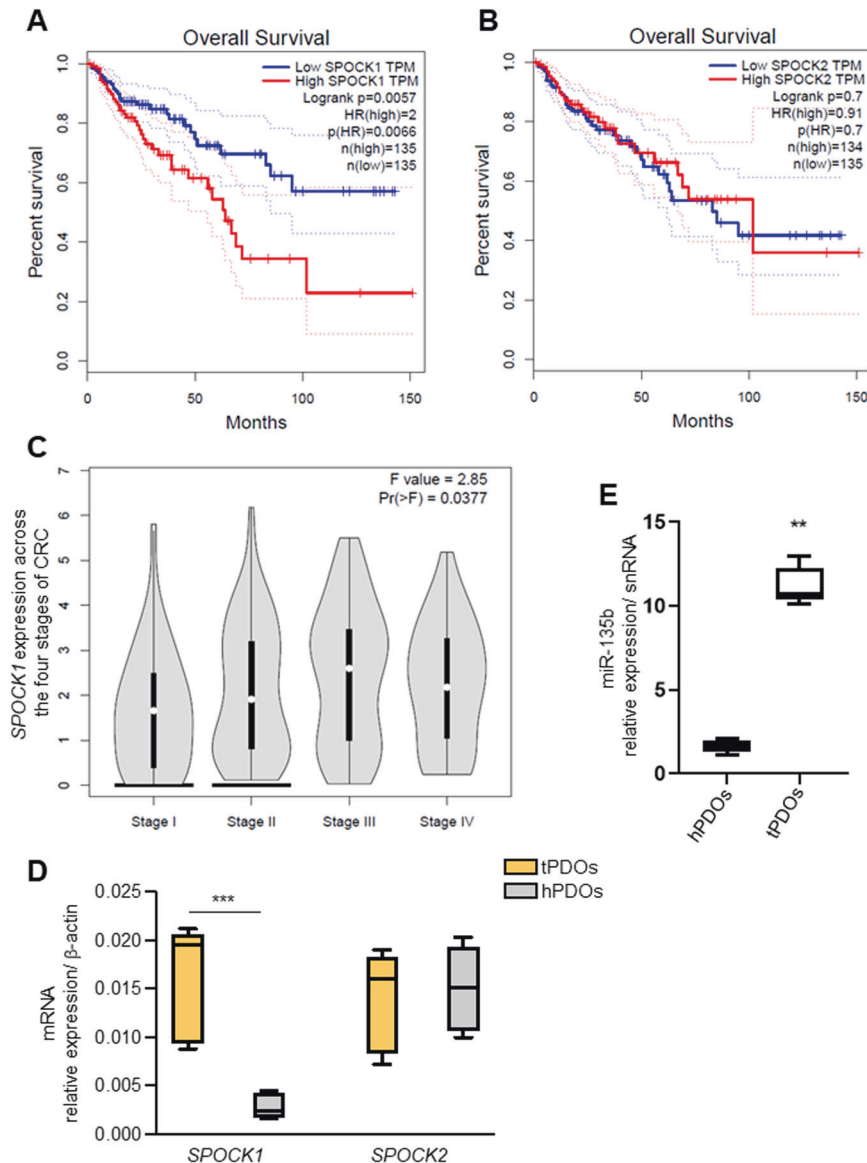


Fig. 4 SPOCK1 is highly expressed in the advanced- stage of CRC and CRC tPDOs. **A, B** Kaplan–Meier survival analysis showed that overall survival was significantly associated with lower expression of *SPOCK1* (**A**) in CRC patients but not *SPOCK2* (**B**) expression. **C** *SPOCK1* is differentially expressed across the four stages of CRC, and with the highest level in advanced stages III and IV CRC. **D** The relative mRNA expression of *SPOCK1* and *SPOCK2* detected by qRT-PCR and *SPOCK1* was upregulated in CRC tPDOs compared to CRC hPDOs (****P* < 0.001). **E** Relative expressions of miR-135b-5p was elevated in CRC tPDOs compare to CRC hPDOs (***P* < 0.01).

metabolism towards chemotherapy response. Among other regulatory factors, miRNAs emerge as important metabolic regulators, representing a reliable biomarker and manipulating the expression of specific miRNAs can alter chemotherapeutic drug sensitivity [85–87].

We compared mouse duodenal polyp- versus non-polyp-derived organoids (mPOs vs mNPOs), mutated for intestinal *Apc*

and *Fbxw7* tumour suppressor genes, with mPOs showing elevated lactate and consumption of glucose in the medium. The polymerase chain reaction analysis of *Apc* allele displayed loss of heterozygosity (LOH) of *Apc*⁺ allele only mPOs organoids derived from 3 weeks mutant *Apc*^{Min}*Fbxw7*^{ΔG} mice (Fig. S2). The previously published data by Yamada et al., also reported that the small lesions from the small intestine had lost *Apc*⁺ allele versus

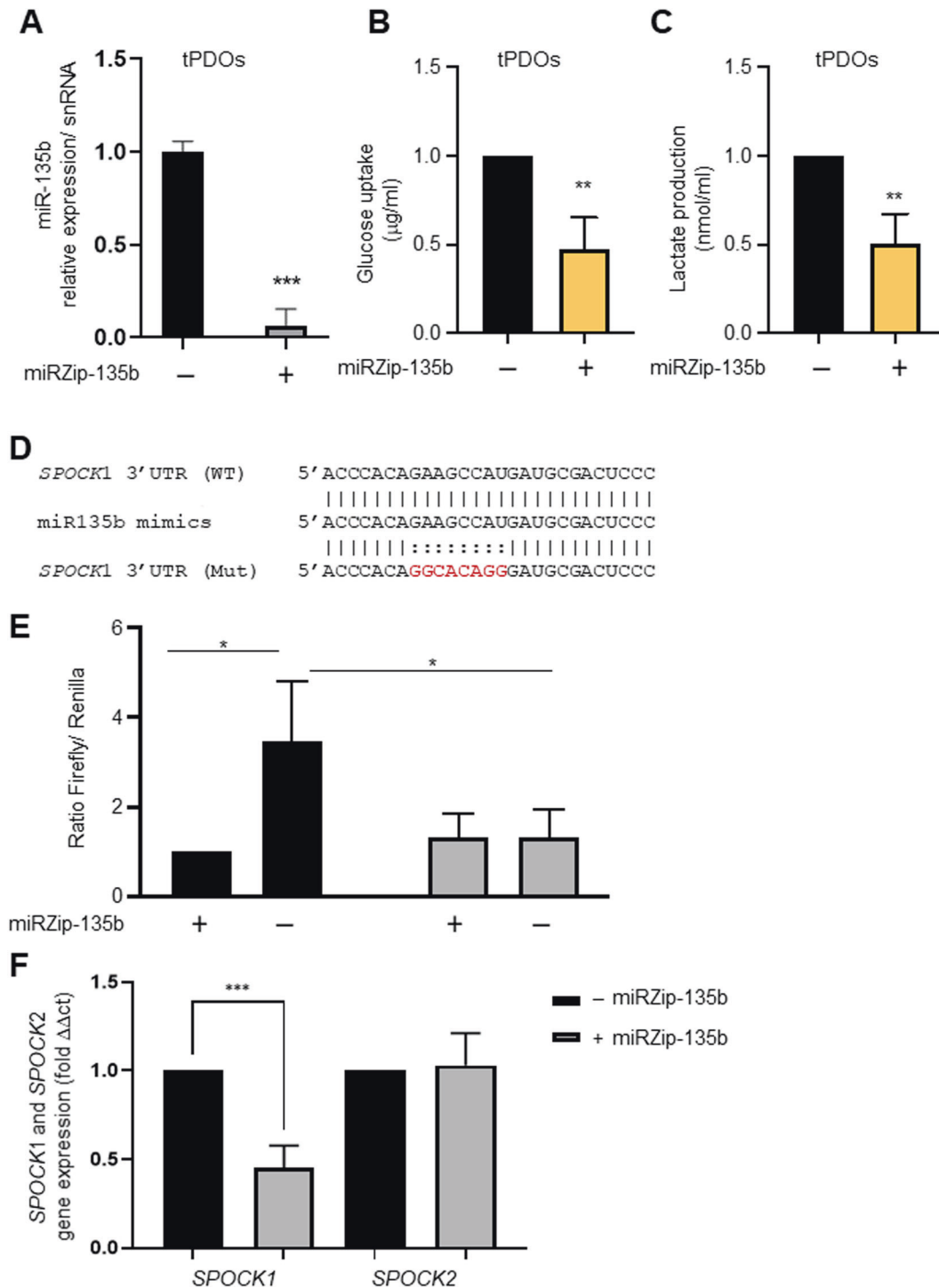


Fig. 5 The miR-135 targets *SPOCK1* gene impact glucose uptake and lactate production in CRC tPDOs. **A** Anti-miR-135 (miRZip-135b) significantly inhibits miR-135 expression in tPDO. **B, C** Anti-miR-135 (miRZip-135b) significantly inhibits glucose uptake and lactate production in tPDO. **D** The sequence of wild type (WT) and mutant (Mut) miR-135b target site in the *SPOCK1* 3'-UTR shown in the frame. A point mutation (highlighted in red) was made in the seed region to block the binding between miR-135b. **E** According to dual-luciferase reporter assay, the relative luciferase activities of DLD-1 cells in *SPOCK1*-WT + Anti-miR-135 (miRZip-135b) was significantly decreased, while in *SPOCK1*-MUT + Anti-miR-135 (miRZip-135b) showed no significant variation (* $P < 0.05$). **F** Anti-miR-135 (miRZip-135b) significantly suppresses the expression *SPOCK1* but not *SPOCK2* in CRC tPDOs.

normal-appearing crypts in *Apc*^{Min/+} model of mice [88]. Such findings suggest that LOH of the *Apc* gene is needed for tumorigenesis in mPOs versus mNPOs. Modelling the duodenal polyp-derived organoids is a close fit observed in the intestine as a whole, including the large bowel [89]. Therefore, mPOs and

mNPOs as models correspond to stimulating aerobic glycolysis in tumours compared with normal adjacent tumour tissues and assessing the level of cellular metabolic changes. In support of this, genes that mediate aerobic glycolysis, including *Aldob*, *Cyba*, *Fabp6*, *Hk2*, *Spoek1* and *Spoek2*, are significantly induced in mPOs

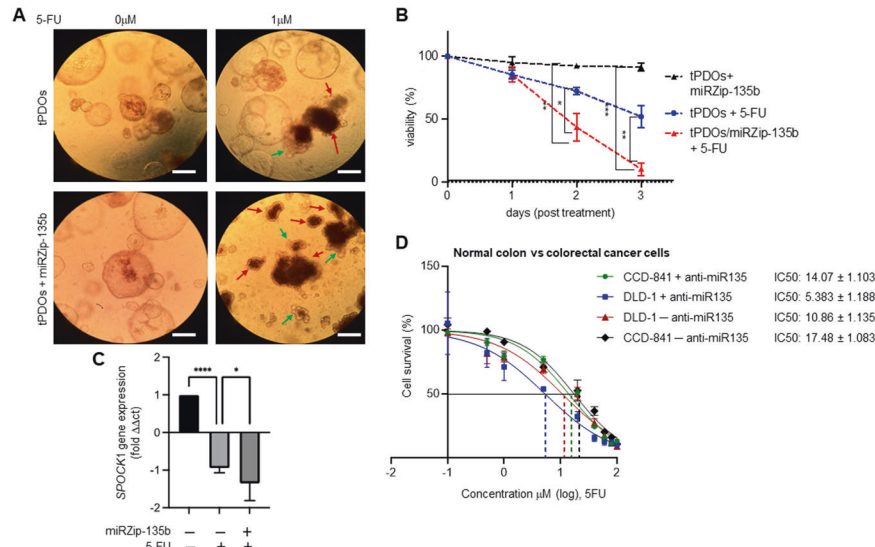


Fig. 6 Knockdown of miR-135b (miRZip-135b) sensitises CRC tPDOs and cells to 5-FU-induced cytostatic and cytotoxicity. **A** Representative images of tPDOs and miR-135b-knockdown (miRZip-135b) tPDOs before (left panels) and after (right panels) 5-FU (1 mM, 48 h) treatment. Arrowheads shows signs and symptoms of possible differentiation (green), morphological, and cytostatic (red) alteration in growth were observed throughout the treatment period. Images were taken using a Leica microscope. Scale bar: 75 μ m. **B** miR-135b-knockdown in tPDOs induced cytostatic (red vs blue) in response to 5-FU (1 mM) determined and quantified by MTT reduction. Bars are \pm SEM ($n = 3$). * $p < 0.05$; ** $p < 0.01$; *** $p < 0.001$. **C** Anti-miR-135b/5-FU axis synergistically prevents SPOCK1 expression in 5-FU-treated CRC tPDOs. **D** Cytotoxicity effect of miR-135b-knockdown on DLD-1 colon cancer cells, and CCD-841 normal colon cells. This experiment was performed in triplicate for each cell line on three independent occasions. IC50 values were calculated by using GraphPad Prism software 7.02.

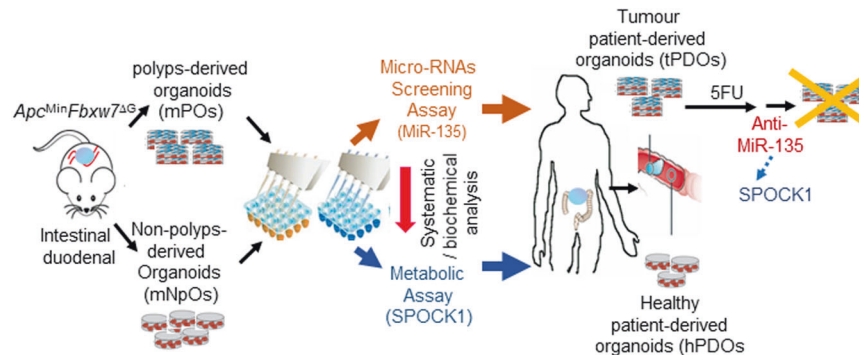


Fig. 7 Graphical abstract and highlights. The tumour and adjacent non-tumour organoids bear differential metabolic activity. Murine *Apc^{Min}Fbxw7^{ΔG}* duodenal polyp-derived organoids mimic colorectal cancer patient-derived organoids. MiR-135b adapts cellular metabolism by targeting *SPOCK1*. MiR-135 and *SPOCK1* synergistically influence tumour cell metabolism and drug response.

compared with mNPOs, which is following the previous report for enriched transcripts in *Apc*-mutant cells [6, 39].

Upregulation of cancer-causing miRNAs, known as oncomiRs, have been found in many types of cancers and, therefore, represents a potential new class of targets for therapeutic inhibition. Several strategies have been developed in recent years for in vivo inhibition of oncomiRs. Hence, in this study, we focused on overexpressed miRNAs. Our miRNAs array findings support our hypothesis that a selected profile miRNAs are significant for the ability of organoid cells to resist drastic changes in their microenvironment. Specifically, we showed that the miR-135 expression induced in mPOs compared with mNPOs, and human CRC tPDOs compared with hPDOs, which increased the expression of *SPOCK1* to induce the cellular glucose consumption. However, in contrast to the general assumption that miRNA-mediated downregulation is a one-way process, miR-135 increased the expression of *SPOCK1*. We could not examine the interaction of miR-135 with *SPOCK1* experimentally; nevertheless, some studies

revealed that miRNAs could activate gene expression directly or indirectly in response to different cell types and conditions and the presence of distinct cofactors. Therefore, further mechanistic studies are required to explore the miR-135-mediated upregulation of *SPOCK1* gene expression [90]. The miR-135 family includes miR-135a and miR-135b isoforms. Although they are located at different chromosomes, the mature miR-135a and miR-135b have only one nucleotide difference, which is not in the miRNA binding region. Thus, it is reported that both isoforms target to same genes [91, 92]. miR-135a and miR-135b were previously shown to be critical in aerobic glycolysis, cancer tumorigenesis, progression, and metastasis in multiple cancer types including CRC [38, 93, 94]. Although there is a possibility that miR-135/ *SPOCK1* axis affects other pathways, our data establish a key role for miR-135 in the regulation of *SPOCK1* homeostasis activity [44], to promote cancer phenotype in murine PO and human tPDOs. As outlined above, several studies recently demonstrated that the knockdown of *SPOCK1* inhibits the

proliferation and invasion of CRC cells [44, 53, 55, 57, 67, 68]. Therefore, our data highlight the therapeutic potential of targeting miR-135/SPOCK1 to enhance the treatment of colorectal cancer (Fig. 7).

MATERIALS AND METHODS

Mouse lines

The double-mutant *Apc*^{Min}*Fbxw7*^{ΔG} mouse was described in [20, 27, 95]. Only the same sex littermates of 2–3-week-old mice were used. Mice were housed and bred in a pathogen-free transgenic animal facility of the Biomedical Service Unit, University of Nottingham. All procedures complied with regulations and guidelines of the Biomedical Service Unit.

Culture of murine intestinal organoids

Intestinal crypts were isolated from the duodenum of *Apc*^{Min}*Fbxw7*^{ΔG} mutant mice and cultured as previously described [27, 95]. In brief, mice were sacrificed by cervical dislocation and the whole intestine excised, cleaned with cold PBS, and opened longitudinally. Under a Stereo/dissecting microscope, duodenal polyps (i.e. collected from >2–3 cm from the polyps/tumour margin, which did not contain poly(tumour) and non-polyps were divided into 1 mm sections and washed with cold PBS several times until PBS became clear. Crypts were released by incubation in 2 mM ethylenediaminetetraacetic acid (EDTA)/phosphate-buffered saline (PBS) for 30 min at 4 °C and purified using a 70 μm cell strainer. Following isolation by centrifuge (300 G for 5 min), crypts counted and were resuspended with Matrigel (BD Biosciences, Oxford, UK), seeded into a 48-well plate and fed with advanced Dulbecco's modified eagle medium (DMEM)/F-12 medium containing; N2 supplement (1×) (Fisher Scientific, 17502048), B27 supplement (1×) (Fisher Scientific, 12585-010), 1 mM/1 N-acetylcysteine (Sigma, A0737), 50 ng/ml epidermal growth factor (Invitrogen), and 10% Noggin and 10% R-spondin1-conditioned medium (in-house) upon solidification of the Matrigel.

Apc loss of heterozygosity (LOH) analysis

We tested the loss of heterozygosity of the *Apc* gene using PCR with mismatched primers, as described previously [96]. Briefly, genomic DNAs were isolated from both duodenal mNPOs and mPOs organoids derived from 3 weeks mutant *Apc*^{Min}*Fbxw7*^{ΔG} mice, the amplification of the *Apc*^{Min} allele resulted in a 155-bp PCR product with one *HindIII* site, whereas the 155-bp product from the *Apc* + allele contained two *HindIII* sites. *HindIII* digestion of PCR-amplified DNA from mNPOs heterozygous tissue resulted in a 123-bp product from the *Apc* + allele and a 144-bp product from the *Apc*^{Min} allele. Therefore, PCR products from mPOs with LOH displayed only one band (144-bp) from the *Apc*^{Min} allele (Fig. S2).

Patient-derived organoids (PDOs) culture and lentivirus infection

The Nottingham Health Science Biobank (NHSB) human tissue ethical approval (REC-15/NW/0685) granted the work, and all the tissues samples were from NHSB. All procedures were conducted following the Declaration of Helsinki and local ethics committee approval. CRC patient-derived organoids (PDOs) were cultured as described in [63, 64]. After 4–5 days incubation, PDOs were incubated with cell recovery solution (Corning) to remove the Matrigel and miRZip-135b anti-miR-135b microRNA constructs (System Biosciences) lentivirus transduction carrying antisense miR-135b (anti-miR-135b). Lentiviral particles were produced by the polyethylenimine (PEI) in 293T packaging cell line and infection was performed as previously described [27, 64]. After infection transduced organoids were treated with 1 μg/ml 5-FU (Tocris) and/or complete organoid medium as vehicle control for their morphology, and live/dead staining. The PDOs were cultured from the colon of a patient with colonic cancer; moderately differentiated adenocarcinoma and TNM staging of T2 N0 M0. The data presented in this study are from three different lines and were assayed at least twice, independently.

Analysis of glucose consumption and lactate production

PO-organoids (murine duodenal *Apc*^{Min}*Fbxw7*^{ΔG}- mPOs vs mNPOs and CRC tPDOs vs hPDOs) were passaged, counted and a similar number of organoids (~200) seeded in six-well culture plate (i.e. P1-organoids) by three independent times. After an additional 48 h of incubation, the media was harvested for measurement of glucose and lactate concentration [38].

According to the manufacturer's instructions, glucose levels with assay kits (Sigma, GAHK20) and the extracellular lactate levels were measured by lactate assay kits (Sigma, MAK065), in the media before (as control) and after the 48 h incubation period within 12 days. The analysis was as followed: glucose uptake = glucose in the medium before the incubation (mM) – glucose in cultured medium (mM); lactate production = lactate in cultured medium (mM) – lactate in the fresh medium (mM). All metabolite measurements were normalised per organoid type.

Organoid viability using MTT assay

After 3 days of culture, the same number of anti-miR-135-transduced organoids were exposed overnight to 1 μg/ml 5-FU for 24 h. Organoids death was determined by 3-(4,5-dimethylthiazol-2-yl)-2,5-diphenyltetrazolium bromide (MTT) reduction as described in [97]. Briefly, after treatment, the MTT solution was added to the organoid culture to a final concentration of 500 μg/ml and incubated at 5% CO₂, 37 °C for 90 min. Then, the medium was replaced with 20 μl of 2% SDS solution in H₂O at 37 °C for 1 h to solubilise the Matrigel. Then, to solubilise the reduced MTT, 100 μl of DMSO was added for 1 h at 37 °C. The absorbance of each well was measured at 562 nm in a plate reader (Bio-Rad).

Cytotoxicity assay

For the cytotoxicity assay, anti-miR-135b lentivirus transduced and untransduced DLD-1 and CCD-841 cells were serum-starved for 18 h and then treated with ten increasing doses of 5-FU (Tocris) for 72 h, and Sulforhodamine-B (SRB) colorimetric assay (Sigma, 230162) was performed as previously described [27, 95].

Real-time PCR

Total RNA was extracted using TRIzol reagent (Sigma, T9424) and miRNeasy kit (QIAGEN, 217004) from mouse intestinal organoids and human CRC PDOs. Fifty nanograms of RNA were reverse transcribed with miScript Reverse Transcription Kit (QIAGEN, 218161). Real-time PCR for selected metabolic genes, and miRNAs (Tables S2 and S3), was performed using SYBR Green master mixes (Applied Biosystems, A46110). All reactions were run in triplicates. Three snRNAs (U6snRNA, SNORD38B and SNORD49A) are regarded reference gene candidates. Normalisation was performed by using the four RNA spike-ins contained in the RNA Spike-in Kit (UniSp2, UniSp4, UniSp5 and cel-miR-39-3p) (QIAGEN). Relative expression was calculated with relative standard curves for miR-135b and the endogenous control. RT-PCR analysis was performed using an ABI Prism 7900 Sequence Detector (Applied Biosystems).

MicroRNA target prediction

TargetScan (<http://www.targetscan.org>) [60], miRDB (<http://mirdb.org/>) [98], miRanda (<http://www.microrna.org>) [99] and miRBase (<http://www.mirbase.org>) [100] were used for miRNAs target identification and prediction.

Western blotting and reporter assay

Western blotting analyses were conducted as previously described [27], with anti-SPOCK1 and anti-SPOCK2 antibodies (ThermoFisher). HEK293T were transiently co-transfected by Lipofectamine 2000 (Life Technologies Corporation) with 0.8 μg of Firefly/Renilla luciferase reporter plasmid (pEZXT06) containing wild type or mutated *SPOCK1* 3'UTRs, corresponding to the miR-135b mimic or control-mutant oligonucleotides (GeneCopoeia). Forty-eight hours post-transfection luciferase activity was quantified by Dual-Luciferase Reporter kit (Promega Inc.) The Luciferase reporter assays were performed in triplicates and HEK293 cells using a multifunction microplate reader (FLUOstar OPTIMA; BMG Labtech). For statistical analysis, the ratio of Firefly-Luc activity to Renilla-Luc was obtained, normalised and data expressed as fold-induction from three independent experiments. Mean ± SD ($n = 3$; $P \leq 0.001$).

Statistical analysis

GraphPad Prism 7 (GraphPad Software, San Diego, CA, USA) and Microsoft Office Excel were used to generate graphs and carry out statistical analysis. Data were reported as means ± SEM using the Student *t*-test, one-way analysis of variance (ANOVA), and the Mann–Whitney *U*-test, as appropriate and for all analyses; $p < 0.05$ was considered statistically significant. * $p < 0.05$; ** $p < 0.01$; *** $p < 0.001$ values are shown.

REFERENCES

- Rodríguez-Colman MJ, Schewe M, Meerlo M, Stigter E, Gerrits J, Pras-Raves M, et al. Interplay between metabolic identities in the intestinal crypt supports stem cell function. *Nature*. 2017;543:424–7.
- Schell JC, Wisidagama DR, Bensard C, Zhao H, Wei P, Tanner J, et al. Control of intestinal stem cell function and proliferation by mitochondrial pyruvate metabolism. *Nat Cell Biol*. 2017;19:1027–36.
- Igarashi M, Guarente L. mTORC1 and SIRT1 cooperate to foster expansion of gut adult stem. *Cells Calor Restriction Cell*. 2016;166:436–50.
- Vousden KH, Ryan KM. p53 and metabolism. *Nat Rev Cancer*. 2009;9:691–700.
- Kimmelman AC. Metabolic dependencies in RAS-driven cancers. *Clin Cancer Res*. 2015;21:1828–34.
- Sandoval IT, Delacruz RG, Miller BN, Hill S, Olson KA, Gabriel AE, et al. A metabolic switch controls intestinal differentiation downstream of Adenomatous polyposis coli (APC). *eLife*. 2017;6:e22706.
- Choi SY, Collins CC, Gout PW, Wang Y. Cancer-generated lactic acid: a regulatory, immunosuppressive metabolite? *J Pathol*. 2013;230:350–5.
- San-Millán I, Brooks GA. Reexamining cancer metabolism: lactate production for carcinogenesis could be the purpose and explanation of the Warburg effect. *Carcinogenesis*. 2017;38:119–33.
- Vander Heiden MG, Cantley LC, Thompson CB. Understanding the Warburg effect: the metabolic requirements of cell proliferation. *Science*. 2009;324:1029–33.
- Aran D, Camarda R, Odegaard J, Paik H, Oskotsky B, Krings G, et al. Comprehensive analysis of normal adjacent to tumor transcriptomes. *Nat Commun*. 2017;8:1077.
- Gerweck LE, Seetharaman K. Cellular pH gradient in tumor versus normal tissue: potential exploitation for the treatment of cancer. *Cancer Res*. 1996;56:1194–8.
- Patkar S, Heselmeyer-Haddad K, Auslander N, Hirsch D, Camps J, Bronder D, et al. Hard wiring of normal tissue-specific chromosome-wide gene expression levels is an additional factor driving cancer type-specific aneuploidies. *Genome Med*. 2021;13:93.
- Gil-Zamorano J, Tomé-Carneiro J, Lopez de Las Hazas MC, Del Pozo-Acebo L, Crespo MC, Gómez-Coronado D, et al. Intestinal miRNAs regulated in response to dietary lipids. *Sci Rep*. 2020;10:18921.
- Ruiz-Roso MB, Gil-Zamorano J, López de Las Hazas MC, Tomé-Carneiro J, Crespo MC, Latasa MJ, et al. Intestinal lipid metabolism genes regulated by miRNAs. *Front Genet*. 2020;11:707.
- McKenna LB, Schug J, Vourekas A, McKenna JB, Bramswig NC, Friedman JR, et al. MicroRNAs control intestinal epithelial differentiation, architecture, and barrier function. *Gastroenterology*. 2010;139:1654–64. 1664.e1651
- Yeh CH, Bellon M, Nicot C. FBXW7: a critical tumor suppressor of human cancers. *Mol Cancer*. 2018;17:115.
- Yumimoto K, Nakayama KI. Recent insight into the role of FBXW7 as a tumor suppressor. *Semin Cancer Biol*. 2020;67:1–15.
- Schell MJ, Yang M, Teer JK, Lo FY, Madan A, Coppola D, et al. A multigene mutation classification of 468 colorectal cancers reveals a prognostic role for APC. *Nat Commun*. 2016;7:11743.
- Markowitz SD, Bertagnoli MM. Molecular origins of cancer: molecular basis of colorectal cancer. *N Engl J Med*. 2009;361:2449–60.
- Babaei-Jadidi R, Li N, Saadeddin A, Spencer-Dene B, Jandke A, Muhammad B, et al. FBXW7 influences murine intestinal homeostasis and cancer, targeting Notch, Jun, and DEK for degradation. *J Exp Med*. 2011;208:295–312.
- Davis H, Lewis A, Behrens A, Tomlinson I. Investigation of the atypical FBXW7 mutation spectrum in human tumours by conditional expression of a heterozygous propellor tip missense allele in the mouse intestines. *Gut*. 2014;63:792–9.
- Sancho R, Jandke A, Davis H, Diefenbacher ME, Tomlinson I, Behrens A. F-box and WD repeat domain-containing 7 regulates intestinal cell lineage commitment and is a haploinsufficient tumor suppressor. *Gastroenterology*. 2010;139:929–41.
- Nateri AS, Spencer-Dene B, Behrens A. Interaction of phosphorylated c-Jun with TCF4 regulates intestinal cancer development. *Nature*. 2005;437:281–5.
- Welcker M, Orian A, Jin J, Grim JE, Harper JW, Eisenman RN, et al. The Fbw7 tumor suppressor regulates glycogen synthase kinase 3 phosphorylation-dependent c-Myc protein degradation. *Proc Natl Acad Sci USA*. 2004;101:9085–90.
- Nateri AS, Riera-Sans L, Da Costa C, Behrens A. The ubiquitin ligase SCFFbw7 antagonizes apoptotic JNK signaling. *Science*. 2004;303:1374–8.
- Wertz IE, et al. Sensitivity to antitubulin chemotherapeutics is regulated by MCL1 and FBW7. *Nature*. 2011;471:110–4.
- Li N, Babaei-Jadidi R, Lorenzi F, Spencer-Dene B, Clarke P, Domingo E, et al. An FBXW7-ZEB2 axis links EMT and tumour microenvironment to promote colorectal cancer stem cells and chemoresistance. *Oncogenesis*. 2019;8:13.
- Gupta-Rossi N, Le Bail O, Gonen H, Brou C, Logeat F, Six E, et al. Functional interaction between SEL-10, an F-box protein, and the nuclear form of activated Notch1 receptor. *J Biol Chem*. 2001;276:34371–8.
- Cassavaugh JM, Hale SA, Wellman TL, Howe AK, Wong C, Lounsbury KM. Negative regulation of HIF-1 α by an FBW7-mediated degradation pathway during hypoxia. *J Cell Biochem*. 2011;112:3882–90.
- Zhang Y, Guo L, Li Y, Feng GH, Teng F, Li W, et al. MicroRNA-494 promotes cancer progression and targets adenomatous polyposis coli in colorectal cancer. *Mol Cancer*. 2018;17:1.
- Middendorp S, Schneeberger K, Wiegerinck CL, Mokry M, Akkerman RD, van Wijngaarden S, et al. Adult stem cells in the small intestine are intrinsically programmed with their location-specific function. *Stem Cells*. 2014;32:1083–91.
- Yilmaz ÖH, Katajisto P, Lamming DW, Gültekin Y, Bauer-Rowe KE, Sengupta S, et al. mTORC1 in the Paneth cell niche couples intestinal stem-cell function to calorie intake. *Nature*. 2012;486:490–5.
- Kwon IG, Kang CW, Park JP, Oh JH, Wang EK, Kim TY, et al. Serum glucose excretion after Roux-en-Y gastric bypass: a potential target for diabetes treatment. *Gut*. 2021;10:1847–56.
- Goldspink DA, Lu VB, Miedzybrodzka EL, Smith CA, Foreman RE, Billing LJ, et al. Labeling and characterization of human GLP-1-secreting L-cells in primary ileal organoid culture. *Cell Rep*. 2020;31:107833.
- Okkelman IA, Neto N, Papkovsky DB, Monaghan MG, Dmitriev RI. A deeper understanding of intestinal organoid metabolism revealed by combining fluorescence lifetime imaging microscopy (FLIM) and extracellular flux analyses. *Redox Biol*. 2020;30:101420.
- Hasan NM, Johnson KF, Yin J, Baetz NW, Fayad L, Sherman V, et al. Intestinal stem cell-derived enteroids from morbidly obese patients preserve obesity-related phenotypes: elevated glucose absorption and gluconeogenesis. *Mol Metab*. 2021;44:101129.
- Esen E, Chen J, Karner CM, Okunade AL, Patterson BW, Long F. WNT-LRP5 signaling induces Warburg effect through mTORC2 activation during osteoblast differentiation. *Cell Metab*. 2013;17:745–55.
- Yang Y, Ishak Gabra MB, Hanse EA, Lowman XH, Tran TQ, Li H, et al. MiR-135 suppresses glycolysis and promotes pancreatic cancer cell adaptation to metabolic stress by targeting phosphofructokinase-1. *Nat Commun*. 2019;10:809.
- Leclerc D, Deng L, Trasler J, Rozen R. ApcMin/+ mouse model of colon cancer: gene expression profiling in tumors. *J Cell Biochem*. 2004;93:1242–54.
- Yang K, Kurihara N, Fan K, Newmark H, Rigas B, Bancroft L, et al. Dietary induction of colonic tumors in a mouse model of sporadic colon cancer. *Cancer Res*. 2008;68:7803–10.
- Bu P, Chen KY, Xiang K, Johnson C, Crown SB, Rakhilin N, et al. Aldolase B-mediated fructose metabolism drives metabolic reprogramming of colon cancer liver metastasis. *Cell Metab*. 2018;27:1249–62.
- oster JD, Wiedemann JM, Pan CJ, Chou JY, Nordlie RC. Discriminant responses of the catalytic unit and glucose 6-phosphate transporter components of the hepatic glucose-6-phosphatase system in Ehrlich ascites-tumor-bearing mice. *Arch Biochem Biophys*. 2001;393:117–22.
- Pedersen PL, Mathupala S, Rempel A, Geschwind JF, Ko YH. Mitochondrial bound type II hexokinase: a key player in the growth and survival of many cancers and an ideal prospect for therapeutic intervention. *Biochim Biophys Acta*. 2002;10:1–3.
- Ye Z, Chen J, Hu X, Yang S, Xuan Z, Lu X, et al. SPOCK1: a multi-domain proteoglycan at the crossroads of extracellular matrix remodeling and cancer development. *Am J Cancer Res*. 2020;10:3127–37.
- Sansom OJ, Mansergh FC, Evans MJ, Wilkins JA, Clarke AR. Deficiency of SPARC suppresses intestinal tumorigenesis in APCMin/+ mice. *Gut*. 2007;56:1410–4.
- Rodríguez-Fleming GH, Fernandes GMM, Russo A, Biselli-Chicote PM, Netinho JG, Pavarino ÉC, et al. Molecular evaluation of glutathione S transferase family genes in patients with sporadic colorectal cancer. *World J Gastroenterol*. 2018;24:4462–71.
- Powell JA, Gardner AE, Bais AJ, Hinze SJ, Baker E, Whitmore S, et al. Sequencing, transcript identification, and quantitative gene expression profiling in the breast cancer loss of heterozygosity region 16q24.3 reveal three potential tumor-suppressor genes. *Genomics*. 2002;80:303–10.
- Harris TR, Hammock BD. Soluble epoxide hydrolase: gene structure, expression and deletion. *Gene*. 2013;526:61–74.
- Kanamoto R, Azuma N, Suda H, Saeki T, Tsuchihashi Y, Iwami K. Elimination of Na⁺-dependent bile acid transporter from small intestine by ileum resection increases [correction of increase] colonic tumorigenesis in the rat fed deoxycholic acid. *Cancer Lett*. 1999;145:115–20.
- Koepsell H. Glucose transporters in the small intestine in health and disease. *Pflug Arch*. 2020;472:1207–48.

51. Merigo F, Brandolese A, Facchin S, Missaggia S, Bernardi P, Boschi F, et al. Glucose transporter expression in the human colon. *World J Gastroenterol*. 2018;24:775–93.
52. Barone S, Fussell SL, Singh AK, Lucas F, Xu J, Kim C, et al. Slc2a5 (Glut5) is essential for the absorption of fructose in the intestine and generation of fructose-induced hypertension. *J Biol Chem*. 2009;284:5056–66.
53. Miao L, Wang Y, Xia H, Yao C, Cai H, Song Y. SPOCK1 is a novel transforming growth factor- β target gene that regulates lung cancer cell epithelial-mesenchymal transition. *Biochem Biophys Res Commun*. 2013;440:792–7.
54. Wang T, Liu X, Tian Q, Liang T, Chang P. Reduced SPOCK1 expression inhibits non-small cell lung cancer cell proliferation and migration through Wnt/ β -catenin signaling. *Eur Rev Med Pharm Sci*. 2018;22:637–44.
55. Shu YJ, Weng H, Ye YY, Hu YP, Bao RF, Cao Y, et al. SPOCK1 as a potential cancer prognostic marker promotes the proliferation and metastasis of gallbladder cancer cells by activating the PI3K/AKT pathway. *Mol Cancer*. 2015;14:12.
56. Veenstra VL, Damhofer H, Waasdorp C, Steins A, Kocher HM, Medema JP, et al. Stromal SPOCK1 supports invasive pancreatic cancer growth. *Mol Oncol*. 2017;11:1050–64.
57. Zhang J, Zhi X, Shi S, Tao R, Chen P, Sun S, et al. SPOCK1 is up-regulated and promotes tumor growth via the PI3K/AKT signaling pathway in colorectal cancer. *Biochem Biophys Res Commun*. 2017;482:870–6.
58. Li Z, Bai P, Peng D, Wang H, Guo Y, Jiang Y, et al. Screening and confirmation of microRNA markers for distinguishing between menstrual and peripheral blood. *Forensic Sci Int Genet*. 2017;30:24–33.
59. Forero DA, González-Giraldo Y, Castro-Vega LJ, Barreto GE. qPCR-based methods for expression analysis of miRNAs. *Biotechniques*. 2019;67:192–9.
60. Agarwal V, et al. Predicting effective microRNA target sites in mammalian mRNAs. *eLife*. 2015;12:05005.
61. Valeri N, Braconi C, Gasparini P, Murgia C, Lampis A, Paulus-Hock V, et al. MicroRNA-135b promotes cancer progression by acting as a downstream effector of oncogenic pathways in colon cancer. *Cancer Cell*. 2014;25:469–83.
62. Wu CW, Ng SC, Dong Y, Tian L, Ng SS, Leung WW, et al. Identification of microRNA-135b in stool as a potential noninvasive biomarker for colorectal cancer and adenoma. *Clin Cancer Res*. 2014;20:2994–3002.
63. Kashfi SMH, Almozayn S, Jinks N, Koo BK, Nateri AS. Morphological alterations of cultured human colorectal matched tumour and healthy organoids. *Oncotarget*. 2018;9:10572–84.
64. Ahmed M, Jinks N, Babaei-Jadidi R, Kashfi H, Castellanos-Urbe M, May ST, et al. Repurposing antibacterial AM404 as a potential anticancer drug for targeting colorectal cancer stem-like cells. *Cancers*. 2019;12:106.
65. Vlachogiannis G, Hedayat S, Vatsioulas A, Jamin Y, Fernández-Mateos J, Khan K, et al. Patient-derived organoids model treatment response of metastatic gastrointestinal cancers. *Science*. 2018;359:920–6.
66. Flood M, Narasimhan V, Wilson K, Lim WM, Ramsay R, Michael M, et al. Patient-derived organoids can predict response to chemotherapy in metastatic colorectal cancer patients. *Sci Transl Med*. 2019;11:eaay2574.
67. Sun LR, Li SY, Guo QS, Zhou W, Zhang HM. SPOCK1 involvement in epithelial-to-mesenchymal transition: a new target in cancer therapy? *Cancer Manag Res*. 2020;12:3561–9.
68. Yang J, Yang Q, Yu J, Li X, Yu S, Zhang X. SPOCK1 promotes the proliferation, migration and invasion of glioma cells through PI3K/AKT and Wnt/ β -catenin signaling pathways. *Oncol Rep*. 2016;35:3566–76.
69. Qin Y, Li L, Wang F, Zhou X, Liu Y, Yin Y, et al. Knockdown of Mir-135b sensitizes colorectal cancer cells to oxaliplatin-induced apoptosis through increase of FOXO1. *Cell Physiol Biochem*. 2018;48:1628–37.
70. Liu B, Liu Y, Zhao L, Pan Y, Shan Y, Li Y, et al. Upregulation of microRNA-135b and microRNA-182 promotes chemoresistance of colorectal cancer by targeting ST6GALNAC2 via PI3K/AKT pathway. *Mol Carcinogenesis*. 2017;56:2669–80.
71. Vander Heiden MG, DeBerardinis RJ. Understanding the intersections between metabolism and cancer biology. *Cell*. 2017;168:657–69.
72. Pavlova NN, Thompson CB. The emerging hallmarks of cancer metabolism. *Cell Metab*. 2016;23:27–47.
73. Li L, Li X, Zhong W, Yang M, Xu M, Sun Y, et al. Gut microbiota from colorectal cancer patients enhances the progression of intestinal adenoma in Apc(min/+) mice. *EBioMedicine*. 2019;48:301–15.
74. Toda K, Kawada K, Iwamoto M, Inamoto S, Sasazuki T, Shirasawa S, et al. Metabolic alterations caused by KRAS mutations in colorectal cancer contribute to cell adaptation to glutamine depletion by upregulation of asparagine synthetase. *Neoplasia*. 2016;18:654–65.
75. La Vecchia S, Sebastián C. Metabolic pathways regulating colorectal cancer initiation and progression. *Semin Cell Dev. Biol*. 2020;98:63–70.
76. Jones CL, Inguva A, Jordan CT. Targeting energy metabolism in cancer stem cells: progress and challenges in leukemia and solid tumors. *Cell Stem Cell*. 2021;28:378–93.
77. Peng J, Cui Y, Xu S, Wu X, Huang Y, Zhou W, et al. Altered glycolysis results in drug-resistant in clinical tumor therapy. *Oncol Lett*. 2021;21:369.
78. Xiao Z, Dai Z, Locasale JW. Metabolic landscape of the tumor microenvironment at single cell resolution. *Nat Commun*. 2019;10:3763.
79. Davis RJ, Gönen M, Margineantu DH, Handeli S, Swanger J, Hoellerbauer P, et al. Pan-cancer transcriptional signatures predictive of oncogenic mutations reveal that Fbw7 regulates cancer cell oxidative metabolism. *Proc Natl Acad Sci USA*. 2018;115:5462–7.
80. Ji S, Qin Y, Liang C, Huang R, Shi S, Liu J, et al. FBW7 (F-box and WD repeat domain-containing 7) negatively regulates glucose metabolism by targeting the c-Myc/TXNIP (thioredoxin-binding protein) axis in pancreatic cancer. *Clin Cancer Res*. 2016;22:3950–60.
81. Pate KT, Stringari C, Sprowl-Tanio S, Wang K, TeSlaa T, Hovetter NP, et al. Wnt signaling directs a metabolic program of glycolysis and angiogenesis in colon cancer. *EMBO J*. 2014;33:1454–73.
82. Stine ZE, Walton ZE, Altman BJ, Hsieh AL, Dang CV. MYC, metabolism, and cancer. *Cancer Discov*. 2015;5:1024–39.
83. Satoh K, Yachida S, Sugimoto M, Oshima M, Nakagawa T, Akamoto S, et al. Global metabolic reprogramming of colorectal cancer occurs at adenoma stage and is induced by MYC. *Proc Natl Acad Sci USA*. 2017;114:E7697–E7706.
84. Saxton RA, Sabatini DM. mTOR signaling in growth, metabolism, and disease. *Cell*. 2017;168:960–76.
85. Pedroza-Torres A, Romero-Córdoba SL, Justo-Garrido M, Salido-Guadarrama I, Rodríguez-Bautista R, Montaña S, et al. MicroRNAs in tumor cell metabolism: roles and therapeutic opportunities. *Front Oncol*. 2019;9:1404.
86. Si W, Shen J, Zheng H, Fan W. The role and mechanisms of action of microRNAs in cancer drug resistance. *Clin Epigenetics*. 2019;11:25.
87. Rupaimoole R, Slack FJ. MicroRNA therapeutics: towards a new era for the management of cancer and other diseases. *Nat Rev Drug Discov*. 2017;16:203–22.
88. Yamada Y, Hata K, Hirose Y, Hara A, Sugie S, Kuno T, et al. Microadenomatous lesions involving loss of Apc heterozygosity in the colon of adult Apc(Min/+) mice. *Cancer Res*. 2002;62:6367–70.
89. Kasendra M, Luc R, Yin J, Manatakis DV, Kulkarni G, Lucchesi C, et al. Duodenum intestine-chip for preclinical drug assessment in a human relevant model. *eLife*. 2020;9:e510135.
90. Ayla VO, Mina R, Kazemzadeh-Bavili S. Mechanisms of miRNA-Mediated Gene Regulation from Common Downregulation to mRNA-Specific Upregulation. *Int J Genom*. 2014;1–15. <https://doi.org/10.1155/2014/970607>.
91. Petracco R, Grechukhina O, Popkhadze S, Massasa E, Zhou Y, Taylor HS. MicroRNA 135 regulates HOXA10 expression in endometriosis. *J Clin Endocrinol Metab*. 2011;96:E1925–33.
92. Issler O, Haramati S, Paul ED, Maeno H, Navon I, Zwang R, et al. MicroRNA 135 is essential for chronic stress resiliency, antidepressant efficacy, and intact serotonergic activity. *Neuron*. 2014;83:344–60.
93. Nagel R, le Sage C, Diosdado B, van der Waal M, Oude Vrielink JA, Bolijn A, et al. Regulation of the adenomatous polyposis coli gene by the miR-135 family in colorectal cancer. *Cancer Res*. 2008;68:5795–802.
94. Taipaleenmäki H, Browne G, Akech J, Zustin J, van Wijnen AJ, Stein JL, et al. Targeting of Runx2 by miR-135 and miR-203 impairs progression of breast cancer and metastatic bone disease. *Cancer Res*. 2015;75:1433–44.
95. Lorenzi F, Babaei-Jadidi R, Sheard J, Spencer-Dene B, Nateri AS. Fbxw7-associated drug resistance is reversed by induction of terminal differentiation in murine intestinal organoid culture. *Mol Ther Methods Clin Dev*. 2016;3:16024.
96. Luongo C, Moser AR, Gledhill S, Dove WF. Loss of Apc+ in intestinal adenomas from Min mice. *Cancer Res*. 1994;54:5947–52.
97. Grabinger T, Luks L, Kostadinova F, Zimmerlin C, Medema JP, Leist M, et al. Ex vivo culture of intestinal crypt organoids as a model system for assessing cell death induction in intestinal epithelial cells and enteropathy. *Cell Death Dis*. 2014;5:e1228.
98. Wong N, Wang X. miRDB: an online resource for microRNA target prediction and functional annotations. *Nucleic Acids Res*. 2015;43:5.
99. Enright AJ, John B, Gaul U, Tuschl T, Sander C, Marks DS. MicroRNA targets in Drosophila. *Genome Biol*. 2003;5:2003–5.
100. Kozomara A, Birgaouan M, Griffiths-Jones S. miRBase: from microRNA sequences to function. *Nucleic Acids Res*. 2019;47:D155–62.

ACKNOWLEDGEMENTS

This work was supported by the Medical Research Council (grant number MR/K00414X/1); and Arthritis Research UK (grant number 19891), and grants from Cancer Research UK (grant numbers A9275, A10247) to ASN and DL; University of Jeddah (grant number UJ-02-019-ICGR) to WA; the Mayor of Gedling's Charitable Grant to DL and the University of Nottingham, UK.

AUTHOR CONTRIBUTIONS

RB-J, WA, SWK, OAM and ASN conceived the project and designed the research and RB-J, HK and AKB performed the experiments, established the systematic and computational analysis, with contributions from AM, and DNL helped with patients samples and advice during the project. RB-J, HK and AKB prepared the manuscript, and ASN participated in study conception, design, and supervision, and ASN and DNL revised the article critically. All authors have read, reviewed and agreed to the published version of the manuscript.

COMPETING INTERESTS

The authors declare no competing interests.

ADDITIONAL INFORMATION

Supplementary information The online version contains supplementary material available at <https://doi.org/10.1038/s41389-021-00376-1>.

Correspondence and requests for materials should be addressed to Abdolrahman S. Nateri.

Reprints and permission information is available at <http://www.nature.com/reprints>

Publisher's note Springer Nature remains neutral with regard to jurisdictional claims in published maps and institutional affiliations.



Open Access This article is licensed under a Creative Commons Attribution 4.0 International License, which permits use, sharing, adaptation, distribution and reproduction in any medium or format, as long as you give appropriate credit to the original author(s) and the source, provide a link to the Creative Commons license, and indicate if changes were made. The images or other third party material in this article are included in the article's Creative Commons license, unless indicated otherwise in a credit line to the material. If material is not included in the article's Creative Commons license and your intended use is not permitted by statutory regulation or exceeds the permitted use, you will need to obtain permission directly from the copyright holder. To view a copy of this license, visit <http://creativecommons.org/licenses/by/4.0/>.

© The Author(s) 2022